Journal Name

ARTICLE

Efficient crystallization-induced emission in fluorenyl-tethered carboranes†

Received 00th January 20xx,
Accepted 00th January 20xx

DOI: 10.1039/x0xx00000x

www.rsc.org/

Zhaojin Wang,[a] Tianyu Wang[a], Chi Zhang[a]* and Mark G. Humphrey[a,b]*

Fluorenyl-tethered *o*-carborane derivatives (Fl-Cb) as both mono- and di-aryl Cb assemblies were synthesized from the corresponding alkyne and $B_{10}H_{12}(Et_2S)_2$ in ca. 60% yields. Crystallographic studies of di-aryl examples show rigid head-to-tail or tail-to-tail packing, while for the mono-aryl examples, only loose packing was observed. In solution, the Fl-Cb compounds exhibit strong quenching of their emission, while aggregation in a mixed solvent results in an enhanced, but still weak, emission [0.11 quantum efficiency (Φ)]. Crystallization-induced emission was observed with the di-aryl examples [Φ up to 0.95]. The excitation spectra are broadened, consistent with considerable orbital degeneracy within the crystals. Theoretical calculations suggest that the inherent orbital degeneracy and the highly-ordered crystalline aggregates contribute to the excellent crystallization-induced emission in these Fl-Cb compounds.

Introduction

Carborane derivatives with electron donor-acceptor substituents have attracted considerable interest in recent years, due to their widespread applications in molecular electronics,[1] light-emitting diodes,[2] and nonlinear optics.[3] Compared to carbon-based materials, carboranes possess improved thermal and chemical stabilities and biocompatibility, and the additional prospect of BNCT (boron neutron capture therapy) applications.[4] Luminescence is necessary to achieve many of these applications. *o*-Carborane (Cb, *ortho*-$C_2B_{10}H_{12}$) is characterized by electron-deficiency and highly polarizable σ-aromaticity, and permits electronic interaction with π-conjugated systems,[5] but because of flexibility in cage C–C bonds, Cb derivatives suffer from non-radiative decay during electronic transitions,[6] leading to weak or effectively zero emission. Although intense emission has been reported in solution,[7] a reliable source of highly emissive solid Cb derivatives remains a major challenge.

In previous studies, some Cb derivatives have been reported to glow as solids, due to the suppression of the aforementioned C–C bond flexibility.[7c,8] Moderate to strong emission is achievable from aggregation-induced emission (AIE) or crystallization-induced emission (CIE), by tethering Cb to rigid aromatic chromophores.[9-11] For example, pyrenyl-Cb compounds show excellent photoluminescence (PL) with quantum efficiencies (Φ_{PL}) > 0.8 in the solid state,[12] and anthracenyl-Cb affords a Φ_{PL} value of 0.38 as a crystal,[13] which can be increased to 0.81 on proceeding to Cb-anthracenyl-Cb.[14] However, functionalized anthracene exhibits poor reactivity towards Cb derivatives and effecting functionalization of pyrene is difficult, limiting the further applications of these systems. D-Cb-A triads (D = N-containing donors, A = phenyltriazine) can harvest light with Φ_{PL} up to 0.97,[2b] but AIE/CIE-active examples are lacking, and few structure-property studies exploring emission as a function of extent of aggregation[15] have been promulgated. In view of the ease of modification and the aromaticity of fluorene, we have targeted Fl-Cb (Fl = fluorenyl) analogues as potentially emissive Cb-based materials, and report herein the enhanced emission induced by crystallization exhibited by our initial examples, together with theoretical modelling of highly-ordered crystalline aggregates to rationalize the observed behaviour.

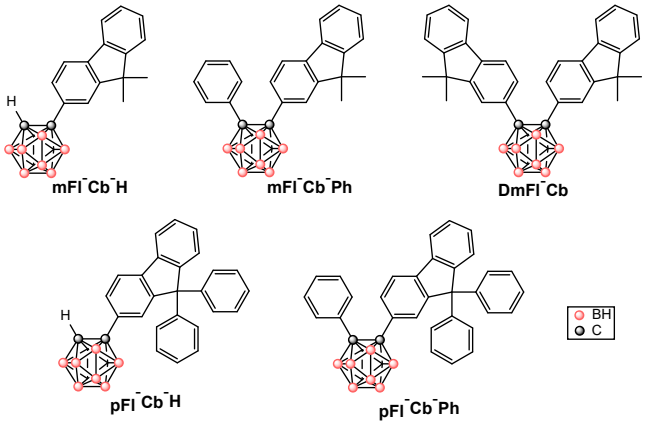

Scheme 1. Structures of Fl-Cb compounds.

[a] *China-Australia Joint Research Centre for Functional Molecular Materials, School of Chemical and Material Engineering, Jiangnan University, Wuxi 214122, P. R. China. E-mail: mark.humphrey@jiangnan.edu.cn*
[b] *Research School of Chemistry, Australian National University, Canberra, ACT 2601, Australia. E-mail: Mark.Humphrey@anu.edu.au*

† Electronic supplementary information (ESI) available: high-resolution mass spectra spectra, crystallographic procedures, crystal packing plots, photophysical studies, TD-DFT-simulated spectra and calculated electronic transitions. CCDC 1527646, 1527647, and 1536124. For ESI and crystallographic data in CIF or other electronic format see DOI: 10.1039/x0xx00000x.

Results and discussion

Previous studies have evidenced large differences in emission of mono- and di-aryl Cb derivatives.[2c,7b,16] As a result of this dependence on the extent of arylation, a systematically-varied range of Fl-Cb examples, including 9,9-dimethylfluorenyl- (mFl)- tethered **mFl-Cb-H**, **mFl-Cb-Ph**, and **DmFl-Cb**, and 9,9-diphenylfluorenyl- (pFl)-tethered **pFl-Cb-H** and **pFl-Cb-Ph**, were synthesized in good yields (Scheme 1: see the Experimental Section for synthesis details).

Crystallography

Figure 1a shows the unit cell from the crystal structure of **mFl-Cb-Ph**, in which two molecules are aligned antiparallel. In each molecule, the carboranyl C–C distance is 1.74 Å and the torsion angle between the C–C bond and mFl is 86.50°, indicative of a large orbital overlap between mFl and Cb.[13] Due to the influence of the Ph, the **mFl-Cb-Ph** molecules are assembled in a "head-to-tail" mode, leading to the construction of linear arrays, as depicted in Figure 2 and ESI Figure S6. The distance between the stacked planes is 5.00 Å for mFl…mFl and 5.19 Å for Ph…Ph, but several B–H and C_{sp3}–H moieties are in the pockets between the planes, so the closest approach between the molecules is 2.86 and 2.97 Å. The carboranyl C–C bond vibration is diminished, due to the sterically restricted environment.

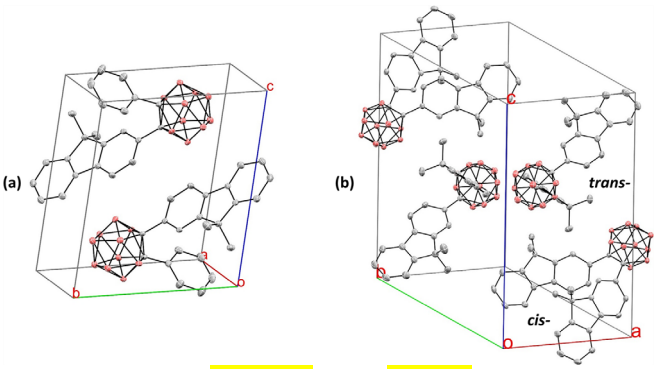

Figure 1. Unit cells of **mFl-Cb-Ph** (a) and **DmFl-Cb** (b). Hydrogens have been omitted for clarity. The *trans*- or *cis*- isomer of **DmFl-Cb** is determined by the relative positions of the methyl groups.

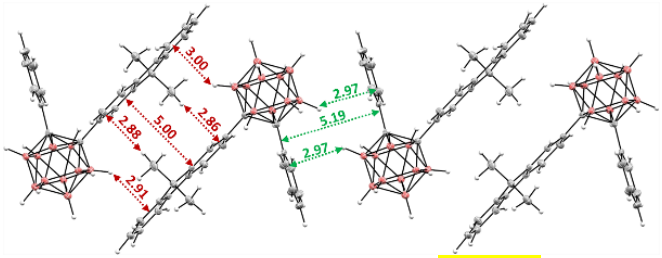

Figure 2. Linear array in the crystal of **mFl-Cb-Ph**. Interplanar mFl…mFl/Cb and Ph…Ph/Cb distances (Å) are labelled in red and green, respectively, and given in Å.

The unit cell of **DmFl-Cb** contains four molecules, which can be categorized as *cis*- and *trans*- conformers (see Figure 1b for definition). In a similar fashion to **mFl-Cb-Ph**, the *cis*-conformers stack to form linear arrays, but with a "tail-to-tail" mode (Figure 3a). The Fl moieties in adjacent molecules maintain interplanar distances of 3.43 Å and 3.52 Å, consistent with the presence of end-to-end π…π interactions (Figures S17-S19). For *trans*-**DmFl-Cb**, the π…π stacking is restricted to a dimeric unit, with a short mFl…mFl interplanar distance of 3.16 Å (Figure 3b). The *trans*-**DmFl-Cb** molecules are embedded in linear arrays of *cis*-**DmFl-Cb** (ESI, Figure S7), leading to restricted mobility of the mFl substituents of both conformers.

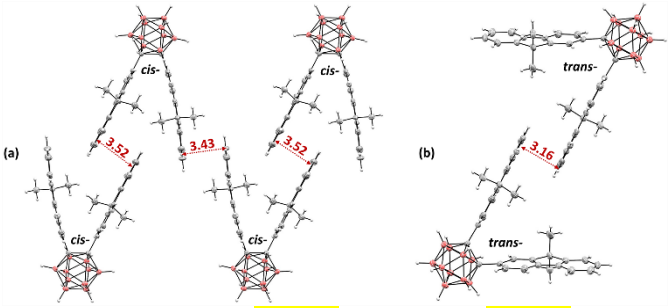

Figure 3. Stacking of *cis*-**DmFl-Cb** (a) and *trans*-**DmFl-Cb** (b). The interplanar mFl…mFl distances are given in Å.

The crystal structure of mono-aryl **pFl-Cb-H** reveals stacking of the **pFl-Cb-H** molecules and was modelled assuming solvent in the lattice voids (ESI, Figure S8). Due to the absence of the additional steric hindrance mentioned above, its carboranyl C–C bond is free to vibrate in the crystal.

Photophysical properties in solution and AIE performance

The photophysical properties of the Fl-Cb compounds were measured in hexane, CH_2Cl_2, and CH_3CN. The absorption spectra of the compounds contain similar bands (Figure 4, left), with a slight red-shift of the band centred in the region 307 to 320 nm for the pFl derivatives; this band corresponds to the lowest π_{Fl}–π^*_{FlCb} transition.[7b] The emission spectra of the di-aryl examples exhibit charge-transfer (CT) emission (Stoke shift > 90 nm), while the mono-aryl examples exhibit only locally-excited emission due to quenching of the CT emission (Figure 4, right). The emission is quenched, with a Φ_{PL} less than 1% in hexane and lower in CH_2Cl_2 or CH_3CN (ESI, Figure S9); non-radiative decay in solution is responsible for this quenching.

The aggregation of the Fl-Cb compounds in mixed solvents was then investigated. **DmFl-Cb** aggregates in CH_3CN/H_2O (V/V= 4:6), with the emission decreasing slightly with increasing water fraction, as seen in Figure 5. The intensity of the aggregation-induced emission is almost one hundred-fold that of the CH_3CN solution, but the resulting maximum emission is still low (Φ_{PL} 11 % with quinine sulfate as standard; see ESI Figure S10).

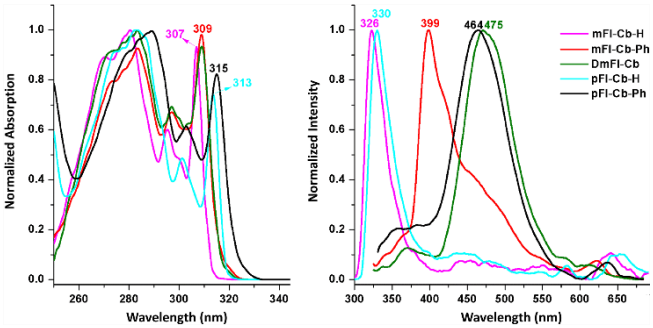

Figure 4. Normalized absorption (left) and emission spectra (right: excitation at 300 nm) of Fl-Cb compounds in hexane.

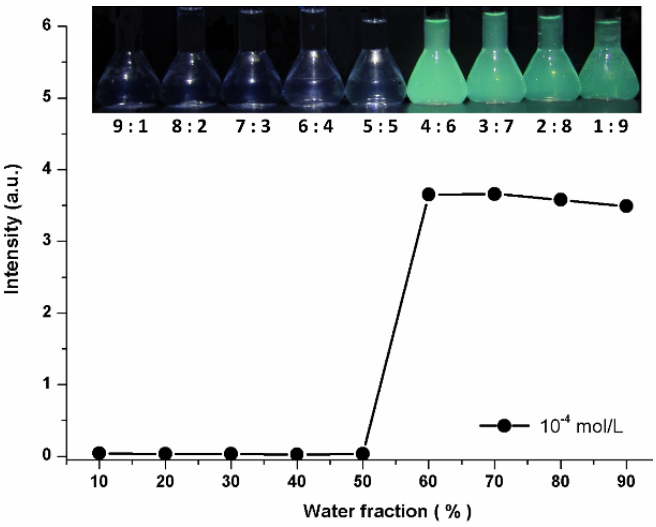

Figure 5. Relative PL intensities of **DmFl-Cb** in CH_3CN/H_2O with varying water fractions. Inset: PL appearance under irradiation at 365 nm with different ratios of CH_3CN/H_2O (V/V).

Enhanced emission in crystals or powder

Upon progressing from solution to the solid, crystalline **mFl-Cb-Ph** and **DmFl-Cb** and powder **pFl-Cb-Ph** undergo significant emission enhancement, while the mono-aryl species **mFl-Cb-H** and **pFl-Cb-H** remain non-emissive (Figure 6, inset). Broadened peaks which are centred around 500 nm and span the wavelength range from 400 to 650 nm are seen in the emission of all the luminous species, while broadened peaks are also seen in the excitations. In the di-aryl examples, excitation maxima are separated by 88 nm for **mFl-Cb-Ph**, 58 nm for **DmFl-Cb**, and 28 nm for **pFl-Cb-Ph**, but in all three cases the wavelengths between the maxima afford emission comparable in intensity to the maximal values. Because excitation occurs with no relaxation, we propose that orbital degeneracies lead to a series of closely separated energy levels inherent in the crystals, as illustrated in Figure 7. Because of this degeneracy, electronic transition occurs with a much lower excitation energy relative to the lowest absorption in solution. The consistent ordering of crystallinity and wavelength range of excitation (**mFl-Cb-Ph** > **DmFl-Cb** > **pFl-Cb-Ph**) reveals that the more ordered aggregation the solid possesses, the larger the orbital degeneracy that it undergoes.

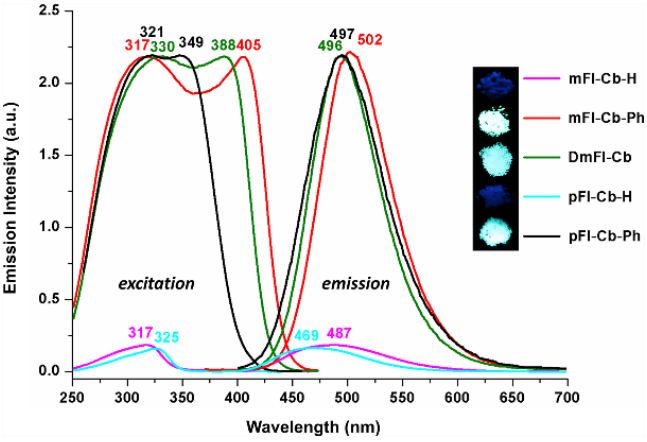

Figure 6. Excitation and emission spectra of Fl-Cb compounds in crystal or powder form. Inset: solid fluorescence in the dark (wavelength of irradiation: 365 nm).

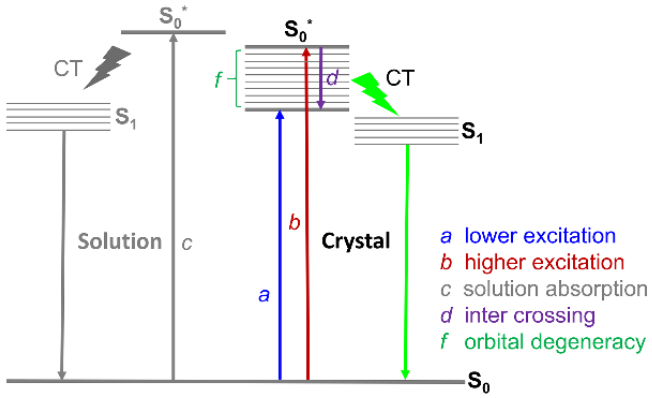

Figure 7. A comparison of electronic transitions of di-aryl Fl-Cb derivatives in solution and in the crystal. S_0, S_0* and S_1 represent the ground state, the original excited state and the charge-separated excited state, respectively.

Table 1. Parameters from PL decay studies of the di-aryl examples

Solid	λ_{ex} [nm]	Φ_{PL}[a]	τ [ns][b]	χ^2
mFl-Cb-Ph	317/405	0.95/0.47	3.824	1.069
DmFl-Cb	330/388	0.75/0.35	3.426	1.120
pFl-Cb-Ph	321/349	0.94/0.87	4.082	1.238

a. evaluated using an integrating sphere; the values before and after / correspond to the λ_{ex}. b. evaluated with 330 nm excitation.

For the emissive di-aryl compounds, the Φ_{PL} and lifetime (τ) have been evaluated (Table 1). Crystalline **mFl-Cb-Ph** harvests light with a Φ_{PL} of 0.95 (excitation at 317 nm) while **DmFl-Cb** is somewhat poorer (Φ_{PL} 0.75 at 330 nm). The Φ_{PL} for the powder **pFl-Cb-Ph** is 0.94 (excitation at 321 nm), probably due to it possessing a similar micro-crystalline structure to **mFl-Cb-Ph**. Interestingly, a lower excitation energy leads to lower Φ_{PL} for **mFl-Cb-Ph** and **DmFl-Cb**, but with a negligible difference for **pFl-Cb-Ph**, which probably derives from significantly fewer accessible degenerate states (S_0*) for the former two examples compared to the latter. Nevertheless, in combination with the afore-mentioned weak solution AIE for the di-aryl compounds, the efficient CIE herein is consistent with orbital

degeneracy offering more energy ladders for decay in the rigid crystal structures, and thereby obviating non-radiative dissipation.

The requirements for CIE are not present with the non-emissive mono-aryl examples; the cage C−C bonds have more flexibility, and the narrow excitation profile is consistent with fewer degenerate states.

Theoretical Calculations

To explore the effect of aggregating the Fl-Cb compounds, theoretical calculations were conducted on the representative **mFl-Cb-Ph** using the wB97xD[17] functional and a 6-31G(d,p) basis set. Figure 8 shows the atomic charges of **mFl-Cb-Ph** from a natural population analysis (NPA). The data suggest that the aromatic C atoms are partially negatively charged and the H atoms, including selected B−H and C_{sp3}−H, are partially positively charged, facilitating electrostatic interactions. Frequency modelling suggests moderate intensity bending vibrations at the Fl and Ph moieties (ESI, Figure S12), thereby producing new dipoles that may strengthen the weak interactions with the adjacent B−Hs or C−Hs.[7c] Limited carboranyl C−C vibrations are possible in the aggregates.

Thermodynamic analysis of the **mFl-Cb-Ph** aggregates reveals a stark difference in the energies of the mFl and Ph stackings. Relative to the monomer, the free-energy change proceeding to the mFl-stacked dimer is -0.95 kcal/mol, whereas the corresponding change for the Ph-stacked dimer is 1.58 kcal/mol (Figure 9), the negative value consistent with a proclivity for aggregation of the mFl moieties. Although the simple combination of mFl- and Ph-stacks is not energetically favourable, a stabilization is seen on proceeding to the trimer (free energy change -0.053 kcal/mol), and so crystallization (with aggregation beyond the calculated trimer) employing such thermodynamically-favourable π-stacking is a not-unexpected outcome.

To further probe the nature of the CIE, computational studies of the excited states of **mFl-Cb-Ph** were undertaken. Initially, we simulated the different excited-state (S_1) structures of the monomer by varying the cage C−C bond lengths in the range from 1.75 Å to 2.30 Å (ESI Figure S13). Although the oscillator strengths of the transitions (S_1 to S_0) corresponding to each structure gradually increase on C−C bond elongation, the extent of the increment is less than 50%; the reduction in molecular vibration is therefore insufficient to account for the CIE. In view of the diversity of repeating units in the crystal, we examined different aggregates from monomer to tetramer. Figure 10 shows the results of modelling the electronic transitions of the tetramer corresponding to the lowest-energy absorption band. The electrons in such an extended system appear to be significantly delocalized, as (for example) seen in the transitions from H-3/H-2 to L/L+1 which are distributed over two molecules. Another significant feature in the tetramer is that higher-lying unoccupied orbitals are close in energy to L (e.g. L+3, 0.057 eV higher), while the difference is around 0.6 eV in the dimer or trimer and 1.2 eV in the monomer. In other words, larger aggregates result in smaller energy gaps. Since the crystal is constructed of much larger aggregates, the energy gap will be even smaller. This density of states means that relaxation from higher-lying excited states can readily proceed via lower excited states and thereby afford emission, rather than a non-radiative decay. This may be a key factor in the remarkable CIE in **mFl-Cb-Ph**. Consistent with this suggestion, the **DmFl-Cb** tetramer shows the same trend, with a small energy gap (< 0.15 eV in a limited system) between the contiguous orbitals, as seen in ESI Table S5.

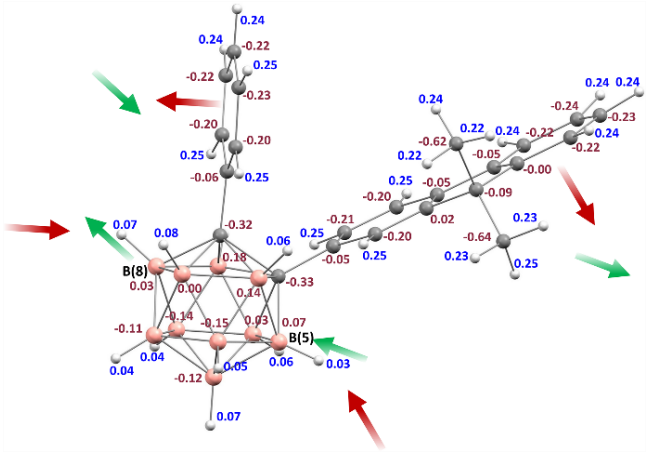

Figure 8. Calculated NPA charges of **mFl-Cb-Ph** and the derived dipoles of bending (for mFl and Ph, red arrows)/stretching (for B−H, green arrows) vibrations. Additional dipoles originate from the vibrations of adjacent molecules.

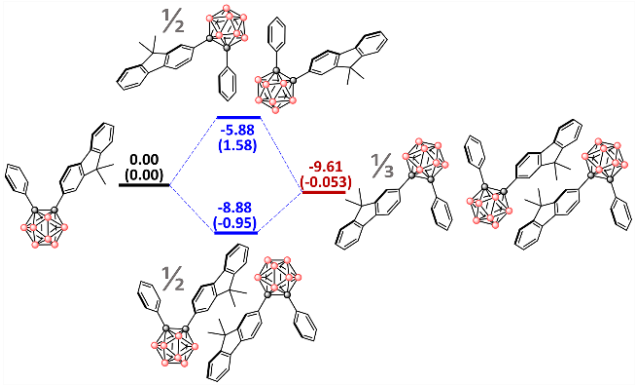

Figure 9. Enthalpy and free energy changes (in parentheses) for different aggregates of **mFl-Cb-Ph**; the values are given in kcal/mol.

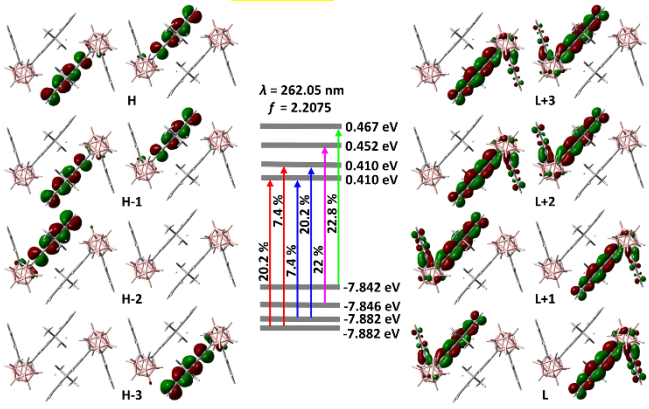

Figure 10. Contributing electronic transitions for the lowest-energy absorption band of the **mFl-Cb-Ph** tetramer. H/L represent the highest-occupied/lowest-unoccupied molecular orbitals.

Conclusion

In summary, we have reported fluorenyl-tethered *o*-carborane derivatives, the three di-aryl analogues exhibiting good crystal-induced emission with quantum efficiencies varying from 0.35 to 0.95. The fluorenyl chromophores have been shown to allow different types of stacking, both leading to the generation of highly-ordered aggregates, with di-aryl substitution leading to diminished carboranyl C–C bond vibration following crystallization. This structural advantage and the extensive orbital degeneracy suggested by the spectroscopic data and corroborated by the theoretical calculations are proposed to be key factors in the enhanced emission. Considering the feasible modifications of the fluorenyl moiety, this study offers new prospects for the design of highly emissive solid *o*-carborane derivatives.

Experimental Section

Materials & Methods

The preparative work was carried out under a nitrogen atmosphere using standard Schlenk techniques. Solvents used for reaction were freshly distilled under nitrogen from either sodium or calcium hydride prior to use. Reactants 6,9-bis(1,1'-thiobis(ethane))decaborane ($B_{10}H_{12}(Et_2S)_2$),[18] 9,9-dimethyl-2-(2-phenylethynyl)-9*H*-Fluorene[19] (**1a**) and 2,2'-(1,2-ethynediyl)bis[9,9-dimethyl-9H-Fluorene][20] (**1c**) were prepared according to literature methods. Other chemicals such as 2-iodo-9,9-dimethylfluorene and 2-bromo-9,9-diphenylfluorene were commercial products and were used as received. The NMR data were obtained on a Bruker DRX 400 spectrometer; chemical shifts are given with respect to $CHCl_3/CDCl_3$ (δ ^{1}H = 7.26 ppm, δ ^{13}C = 77.00 ppm) and external $BF_3{\cdot}Et_2O$ (δ ^{11}B = 0 ppm). Mass spectral data were recorded on Micromass/Waters GCT premier with a high-resolution gas chromatography/time-of-flight mass spectrometer. Elemental analyses were performed on Elementar vario MICRO cube (Germany). The absorption and photoluminescence spectra were recorded on an UV-Vis-NIR spectrophotometer (Shimadzu UV-3600 Plus) and a fluorescence spectrophotometer (Hitachi F-4600) equipped with a high performance R928 photomultiplier detector.

Synthesis of Fluorene-tethered *ortho*-Carborane Derivatives

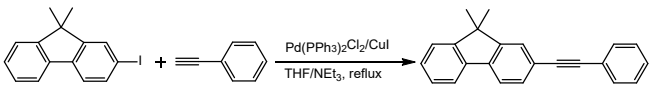

In a 100 mL Schlenk tube, 2-iodo-9,9-dimethylfluorene (4.99 g, 15.6 mmol) and phenylacetylene (2.50 g, 2.69 mL, 24.5 mmol) were dissolved in a mixed solvent of THF/NEt_3 (30 mL/10 mL) and the solution degassed using freeze-pump-thaw cycles. Subsequently, the mixture was frozen and the tube was backfilled with nitrogen. $PdCl_2(PPh_3)_2$ (219 mg, 0.31 mmol) and CuI (119 mg, 0.62 mmol) were added and the N_2 atmosphere was evacuated-backfilled twice. The reaction mixture was then warmed and refluxed for 10 h. After evaporation of the solvent, the residue was purified by silica gel chromatography using hexane as eluent. Recrystallization of the crude product from hot hexane gave **1a** as a colourless solid (4.06 g, yield 88%).

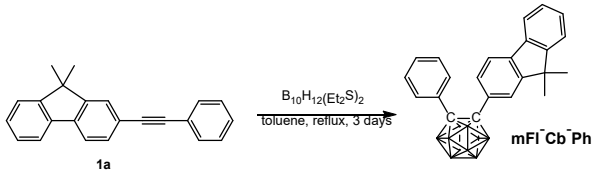

Alkyne **1a** (1.90 g, 6.45 mmol) and $B_{10}H_{12}(Et_2S)_2$ (2.91 g, 9.68 mmol) were dissolved in 30 mL anhydrous toluene, and the resulting mixture was degassed by freeze-pump-thaw. After backfilling with a N_2 flow, the mixture was heated to 110 °C for 3 days. Upon cooling, the unreacted $B_{10}H_{12}(Et_2S)_2$ was quenched by methanol. The solvent was then evaporated under reduced pressure and the residue was passed through a basic alumina column using hexane/CH_2Cl_2 (v/v = 10:1) as eluent. Recrystallization of the crude product from hot ethanol afforded **mFl-Cb-Ph** (1.62 g, 61% yield) as a colorless solid. ^{1}H NMR (400 MHz, $CDCl_3$): δ (ppm) 7.63 (1H, m, Ph), 7.49 (2H, s, Ph), 7.45~7.31 (6H, m, Ph), 7.16 (1H, t, Ph), 7.09 (2H, t, Ph), 4.1~1.6 (10H, br, B–H), 1.27 (6H, s, CH_3); ^{13}C NMR (101 MHz, $CDCl_3$): δ (ppm) 154.08, 153.27, 141.01, 137.56, 130.75, 130.63, 130.25, 130.05, 129.28, 128.17, 127.16, 124.45, 122.66, 120.55, 119.55 (18C, Ph), 85.97 (Cb), 85.34 (Cb), 46.76 ($C(Me)_2$), 26.69 (CH_3); ^{11}B NMR (128 MHz, $CDCl_3$): δ (ppm) -1.91 (1B), -3.00 (1B), -8.68 (2B), -9.89 (4B), -11.00 (2B); HRMS (EI+): *m/z* calcd for $C_{23}H_{28}B_{10}$ 412.3205 (100%), found 412.3224 (100%). Anal. Calcd for $C_{23}H_{28}B_{10}$ (%): C, 66.96; H, 6.84. Found: C, 66.92; H, 6.81.

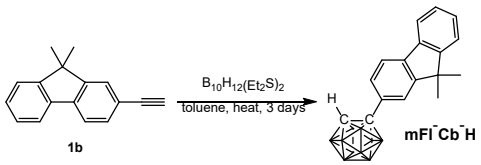

The synthesis of **mFl-Cb-H** followed that of **mFl-Cb-Ph** using alkyne **1b** (1.50 g, 6.87 mmol) and $B_{10}H_{12}(Et_2S)_2$ (3.10 g, 10.3 mmol). Recrystallization of the crude product from hot methanol afforded **mFl-Cb-H** 1.60 g (69% yield) as a white powder. ^{1}H NMR (400 MHz, $CDCl_3$): δ (ppm) 7.72 (1H, m, Ph), 7.64 (1H, d, *J* = 8.0 Hz, Ph), 7.53 (1H, d, J = 2.0 Hz, Ph), 7.46 (2H, m, Ph), 7.37 (1H, d, *J* = 8.0 Hz, Ph), 7.37 (1H, m, Ph), 4.03 (1H, s, C_{Cb}-H), 3.5–1.6 (10H, br, B–H), 1.49 (6H, s, CH_3); ^{13}C NMR (101 MHz, $CDCl_3$): δ (ppm) 154.13, 153.99, 141.08, 137.43, 132.03, 128.29, 127.25, 126.73, 122.70, 122.00, 120.56, 119.95 (12C, Ph), 77.32 (Cb), 60.60 (Cb), 47.08 ($C(CH_3)_2$), 26.96 (CH_3); ^{11}B NMR (128 MHz, $CDCl_3$): δ (ppm) -1.96 (2B), -4.40 (1B), -8.99 (3B), -11.58 (3B), -13.31 (1B). HRMS (EI+): *m/z* calcd for $C_{17}H_{24}B_{10}$ 336.2889 (100%), found for $C_{17}H_{24}B_{10}$ 336.2896 (100%). Anal. Calcd for $C_{17}H_{24}B_{10}$ (%): C, 60.68; H, 7.19. Found: C, 60.60; H, 7.15.

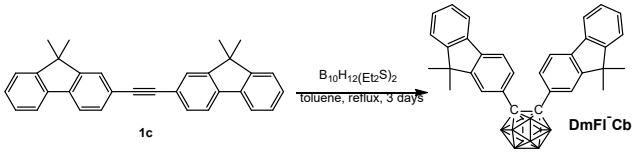

The synthesis of **DmFl-Cb** followed that of **mFl-Cb-Ph** using alkyne **1c** (1.00 g, 2.44 mmol) and $B_{10}H_{12}(Et_2S)_2$ (1.10 g, 3.66 mmol). Recrystallization of the crude product from hot methanol/ ethanol (1:1) afforded **DmFl-Cb** 0.73g (57 %) as a colorless solid. ^{1}H NMR (400 MHz, $CDCl_3$): δ (ppm); 7.56 (2H, m, Ph), 7.47 (2H, dd, J_1 = 8.0 Hz, J_2 = 1.5 Hz, Ph), 7.42 (2H, d, J = 8.0 Hz, Ph), 7.36 (2H, d, J = 1.5 Hz, Ph), 7.26 (6H, m, Ph), 4.0~1.6 (10H, B–H), 1.20 (12H, CH_3); ^{13}C NMR (101 MHz, $CDCl_3$): δ (ppm) 153.97, 153.37, 141.12, 137.43, 130.08, 129.45, 128.12, 127.09, 124.67, 122.56, 120.50, 119.40 (12C, Ph), 86.25 (2C, Cb), 46.71 ($C(Me)_2$), 26.70 (Me); ^{11}B NMR (128 MHz, $CDCl_3$): δ (ppm) -2.16 (1B), -2.93 (1B), -9.92 (5B), -11.13 (3B). HRMS (EI+): *m/z* calcd for $C_{32}H_{36}B_{10}$ 528.3835 (97%), found 528.3839 (100%). Anal. Calcd for $C_{32}H_{36}B_{10}$ (%): C, 72.69; H, 6.86. Found: C, 72.72; H, 6.90.

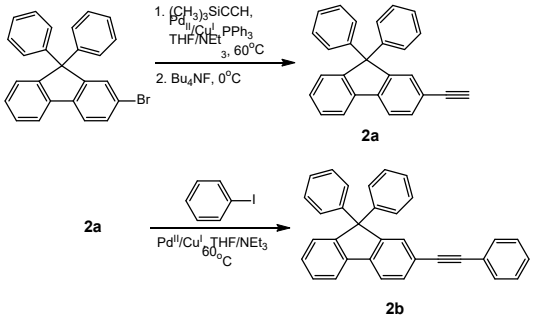

A mixed solvent of THF/NEt_3 (35 mL/15 mL) in a 100 mL Schlenk tube was degassed by freeze-pump-thaw cycles twice and then frozen and backfilled by N_2. 2-Bromo-9,9-diphenylfluorene (4.00 g, 10.1 mmol), $PdCl_2(PPh_3)_2$ (281 mg, 0.40 mmol), CuI (152 mg, 0.80 mmol), PPh_3 (210 mg , 0.80 mmol) were added and the tube was again evacuated-backfilled with N_2. Trimethylsilylacetylene (2.83 mL, 20 mmol) was injected and the reaction mixture was gradually warmed to room temperature and heated to 60°C overnight. Upon cooling, $Bu_4NF{\cdot}3H_2O$ (4.733 g, 15.0 mmol) was added and the mixture was stirred for 2 h. The alkyne **2a** was obtained as a white powder (2.77 g, 81%) after column chromatography. The synthesis of **2b** followed the procedure of **1a** using **2a** (1.50 g, 4.38 mmol) and iodobenzene (0.894 g, 4.38 mmol) as reactants, to give the alkyne **2b** as a white powder (1.57 g, 85%).

2a ^{1}H NMR (400 MHz, $CDCl_3$): δ (ppm) 7.76 (1H, d, J = 7.5 Hz, Ph), 7.72 (1H, d, J = 8.0 Hz, Ph), 7.55 (1H, d, J = 1.5 Hz, Ph), 7.51 (1H, dd, J_1 = 1.5 Hz, J_2 = 8.0 Hz, Ph), 7.42 (1H, d, J = 7.5 Hz, Ph), 7.37 (1H, td, J_1 = 1.0 Hz, J_2 = 7.5 Hz, Ph), 7.29 (1H, td, J_1 = 1.0 Hz, J_2 = 7.5 Hz, Ph), 7.26~7.16 (10H, m, Ph), 3.07 (1H, s, C≡CH); ^{13}C NMR (101 MHz, $CDCl_3$): δ (ppm) 151.53, 151.16, 145.30, 140.86, 139.22, 131.71, 129.92, 128.28, 128.04, 127.61, 126.78, 126.23, 120.96, 120.50, 120.05 (24C, Ph), 84.21 (C≡C), 77.35 (C≡CH), 65.41 (CPh_2). HRMS (EI+): *m/z* calcd for $C_{27}H_{18}$ 342.1408 (100%), found 342.1405 (100%).

2b ^{1}H NMR (400 MHz, $CDCl_3$): δ (ppm) 7.73 (2H, t, J = 7.0 Hz, Ph), 7.55 (1H, s, Ph), 7.52 (1H, d, 8.0 Hz, Ph), 7.48 (2H, m, Ph), 7.39 (1H, d, 8.0 Hz, Ph), 7.37~7.15 (15H, m, Ph); ^{13}C NMR (101 MHz, $CDCl_3$): δ (ppm) 151.61, 151.31, 145.44, 140.39, 139.45, 131.54, 131.24, 129.39, 128.31, 128.30, 128.19, 128.15, 127.62, 126.77, 126.26, 123.27, 122.26, 120.44, 120.12 (30C, Ph), 90.09 (C≡C), 89.66 (C≡C), 65.48 (CPh_2). HRMS (EI+): *m/z* calcd for $C_{33}H_{22}$ 418.1722 (100%), found 418.1720 (100%).

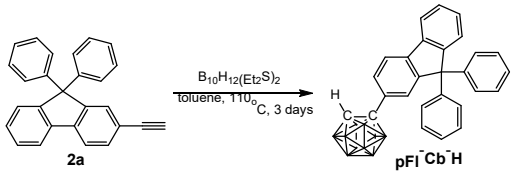

The synthesis of **pFl-Cb-H** followed that of **mFl-Cb-Ph** using alkyne **2a** (1.20 g, 3.50 mmol) and $B_{10}H_{12}(Et_2S)_2$ (1.58 g, 5.26 mmol). After evaporation of solvent, the residue was chromatographed on a basic alumina column using hexane/CH_2Cl_2 (v:v = 6:1) as eluent. Minor impurities were removed by dispersion of the crude product in boiling hexane, affording a white powder of **pFl-Cb-H** (1.05 g, 65%). ^{1}H NMR (400 MHz, $CDCl_3$): δ (ppm) 7.74 (1H, d, J = 7.5 Hz, Ph), 7.65 (1H, d, J = 8.0 Hz, Ph), 7.53 (1H, d, J = 2.0 Hz, Ph), 7.48 (1H, dd, J_1 = 2.0 Hz, J_2 = 8.0 Hz, Ph), 7.39 (1H, d, J = 7.5 Hz, Ph), 7.35 (1H, td, J_1 = 1.0 Hz, J_2 = 7.5 Hz, Ph), 7.30 (1H, td, J_1 = 1.0 Hz, J_2 = 7.5 Hz, Ph), 7.23 (6H, m, Ph), 7.14 (4H, m, Ph), 3.85 (1H, s, C–H), 3.4~1.6 (10H, br, B–H); ^{13}C NMR (101 MHz, $CDCl_3$): δ (ppm) 151.81, 151.58, 145.07, 142.08, 138.37, 132.41, 128.76, 128.44, 127.89, 127.80, 127.28, 127.01, 126.38, 125.86, 120.77, 120.15 (24C, Ph), 77.04 (Cb), 65.63 (CPh_2), 60.59 (Cb); ^{11}B NMR (128 MHz, $CDCl_3$): δ (ppm) -1.94 (d, 1B), -4.34 (1B, br), -9.08 (d, 3B), -11.53 (br, 5B). HRMS (EI+): *m/z* calcd for $C_{27}H_{28}B_{10}$ 460.3207 (99%), found 460.3215 (100%). Anal. Calcd for $C_{27}H_{28}B_{10}$ (%): C, 70.40; H, 6.13. Found: C, 70.35; H, 6.05.

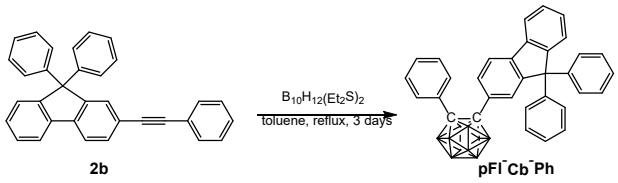

The synthesis of **pFl-Cb-Ph** followed that of **mFl-Cb-Ph** using alkyne **2b** (1.50 g, 3.58 mmol) and $B_{10}H_{12}(Et_2S)_2$ (1.62 g, 5.39 mmol). After evaporation of solvent, the residue was chromatographed on a basic alumina column using hexane/CH_2Cl_2 (v:v = 10:1) as eluent. The targeted product **pFl-Cb-Ph** was obtained as a fluffy white powder (1.21 g, 63%). ^{1}H NMR (400 MHz, $CDCl_3$): δ (ppm) 7.53 (1H, d, J = 7.0 Hz, Ph), 7.53 (1H, s, Ph), 7.40 (2H, s, Ph), 7.29~7.02 (12H, m, Ph), 6.98 (4H, m, Ph), 6.90 (2H, t, J = 7.5 Hz, Ph), 4.0 ~1.5 (10H, br, B–H); ^{13}C NMR (101 MHz, $CDCl_3$): δ (ppm) 151.60, 151.09, 145.04, 142.11, 138.31, 130.40, 130.33, 129.91, 129.51, 128.84, 128.67, 128.31, 128.13, 127.73, 127.63, 126.84, 126.19, 120.77, 119.74 (30C, Ph), 86.06 (Cb), 85.49 (Cb), 65.38 (CPh_2); ^{11}B NMR (128 MHz, $CDCl_3$): δ (ppm) -2.27 (2B), -9.88 (8B). HRMS (EI+): *m/z* calcd for $C_{33}H_{32}B_{10}$

536.3523 (97%), found 536.3520 (100%). Anal. Calcd for $C_{33}H_{32}B_{10}$ (%): C, 73.85; H, 6.01. Found: C, 73.93; H, 5.94.

Computational Details

Density functional theory (DFT) computations were carried out using the Gaussian 09 package.[21] Ground state geometries, including the different degrees of aggregation, were extracted from the crystal structure without further optimization. Molecular orbital modelling and single point energy (SPE) calculations based on these structures were performed with the wB97XD functional using the 6-31G (d, p) basis set for all atoms. Frequency analysis was conducted at the same level of theory to obtain the vibration along with the thermodynamic energy corrections. The excitation energies and oscillator strengths for the lowest 5 singlet–singlet transitions ($S_0 \rightarrow S_1$) from the ground state optimized geometry were obtained by time-dependent (TD)-DFT calculations also using the wB97XD functional and the 6-31G(d, p) basis set. *Note that the excitation energy has been overestimated due to the high content of Hartree-Fock (long-range 100%)*. The S_1 structures with fixed Cb C−C bond length were obtained using "modredundant" criteria under TD-DFT level.

Acknowledgements

We thank the National Natural Science Foundation of China (No. 21502072), the Natural Science Foundation of Jiangsu Province (No. BK20140140), the Chinese Government Ministry of Education and State Administration of Foreign Experts Affairs Program of Introducing Talents of Discipline to Universities (111 Project B13025), and the Australian Research Council for support.

Notes and references

1 (a) R. N. Grimes, *Dalton Trans.*, 2015, **44**, 5939; (b) A. R. Davis, J. J. Peterson and K. R. Carter, *ACS Macro Lett.*, 2012, **1**, 469; (c) J. Marshall, B. C. Schroeder, H. Bronstein, I. Meager, S. Rossbauer, N. Yaacobi-Gross, E. Buchaca-Domingo, T. D. Anthopoulos, N. Stingelin, P. Beavis and M. Heeney, *Macromolecules*, 2014, **47**, 89; (d) A. M. Spokoyny, T. C. Li, O. K. Farha, C. W. Machan, C. She, C. L. Stern, T. J. Marks, J. T. Hupp and C. A. Mirkin, *Angew. Chem. Int. Ed.*, 2010, **49**, 5339; (e) A. Harriman, M. A. Alamiry, J. P. Hagon, D. Hablot and R. Ziessel, *Angew. Chem. Int. Ed.*, 2013, **52**, 6611; (f) M. T. Indelli, T. Bura and R. Ziessel, *Inorg. Chem.*, 2013, **52**, 2918; (g) D. Hablot, A. Sutter, P. Retailleau and R. Ziessel, *Chem. Eur. J.*, 2012, **18**, 1890.

2 (a) K. R. Wee, Y. J. Cho, S. Jeong, S. Kwon, J. D. Lee, I. H. Suh and S. O. Kang, *J. Am. Chem. Soc.*, 2012, **134**, 17982; (b) R. Furue, T. Nishimoto, I. S. Park, J. Lee and T. Yasuda, *Angew. Chem. Int. Ed.*, 2016, **55**, 7171; (c) K. R. Wee, W. S. Han, D. W. Cho, S. Kwon, C. Pac and S. O. Kang, *Angew. Chem. Int. Ed.*, 2012, **51**, 2677.

3 (a) L. Zhu, W. Lv, S. Liu, H. Yan, Q. Zhao and W. Huang, *Chem. Commun.*, 2013, **49**, 10638; (b) F. Nicoud, F. Bolze, X. H. Sun, A. Hayek and P. Baldeck, *Inorg. Chem.*, 2011, **50**, 4272; (c) R. Hamasaki, M. Ito, M. Lamrani, M. Mitsuishi, T. Miyashita and Y. Yamamoto, *J. Mater. Chem.*, 2003, **13**, 21; (d) N. Tsuboya, M. Lamrani, R. Hamasaki, M. Ito, M. Mitsuishi, T. Miyashita and Y. Yamamoto, *J. Mater. Chem.*, 2002, **12**, 2701.

4 (a) M. F. Hawthorne and A. Maderna, *Chem. Rev.*, 1999, **99**, 3421; (b) N. S. Hosmane, *Boron Science: New Technologies and Applications*, CRC Press, Boca Raton, FL, 2011; (c) M. Scholz and E. Hey-Hawkins, *Chem. Rev.*, 2011, **111**, 7035; (d) F. Issa, M. Kassiou and L. M. Rendina, *Chem. Rev.*, 2011, **111**, 5701.

5 (a) R. N. Grimes, *Carboranes*, Academic Press, New York, 2nd edn, 2011; (b) G. F. Jin, J. H. Hwang, J. D. Lee, K. R. Wee, I. H. Suh and S. O. Kang, *Chem. Commun.*, 2013, **49**, 9398.

6 M. Tominaga, H. Naito, Y. Morisaki and Y. Chujo, *New J. Chem.*, 2014, **38**, 5686.

7 (a) K. Kokado, M. Tominaga and Y. Chujo, *Macromol. Rapid Commun.*, 2010, **31**, 1389; (b) Z. Wang, P. Jiang, T. Wang, G. J. Moxey, M. P. Cifuentes, C. Zhang and M. G. Humphrey, *Phys. Chem. Chem. Phys.*, 2016, **18**, 15719; (c) D. Tu, P. Leong, Z. Li, R. Hu, C. Shi, K. Y. Zhang, H. Yan and Q. Zhao, *Chem. Commun.*, 2016, **52**, 12494.

8 (a) K. Kokado, A. Nagai and Y. Chujo, *Macromolecules*, 2010, **43**, 6463; (b) Y. J. Cho, S. Y. Kim, M. Cho, W. S. Han, H. J. Son, D. W. Cho and S. O. Kang, *Phys. Chem. Chem. Phys.*, 2016, **18**, 9702; (c) H. J. Bae, H. Kim, K. M. Lee, T. Kim, Y. S. Lee, Y. Do and M. H. Lee, *Dalton Trans.*, 2014, **43**, 4978.

9 (a) J. Mei, N. L. C. Leung, R. T. K. Kwok, J. W. Y. Lam and B. Z. Tang, *Chem. Rev.*, 2015, **115**, 11718; (b) J. Mei, Y. Hong, J. W. Lam, A. Qin, Y. Tang and B. Z. Tang, *Adv. Mater.*, 2014, **26**, 5429; (c) Y. Hong, J. W. Y. Lam and B. Z. Tang, *Chem. Soc. Rev.*, 2011, **40**, 5361.

10 (a) Y. Dong, J. W. Lam, A. Qin, Z. Li, J. Sun, H. H. Sung, I. D. Williams and B. Z. Tang, *Chem. Commun.*, 2007, 40; (b) P. Galer, R. C. Korosec, M. Vidmar and B. Sket, *J. Am. Chem. Soc.*, 2014, **136**, 7383; (c) S. Ito, A. Hirose, M. Yamaguchi, K. Tanaka and Y. Chujo, *J. Mater. Chem. C*, 2016, **4**, 5564; (d) L. Wang, Z. Zhang, X. Cheng, K. Ye, F. Li, Y. Wang and H. Zhang, *J. Mater. Chem. C*, 2015, **3**, 499; (e) R. Yoshii, A. Hirose, K. Tanaka and Y. Chujo, *J. Am. Chem. Soc.*, 2014, **136**, 18131.

11 (a) L. Weber, J. Kahlert, R. Brockhinke, L. Böhling, A. Brockhinke, H. G. Stammler, B. Neumann, R. A. Harder and M. A. Fox, *Chem. Eur. J.*, 2012, **18**, 8347; (b) S. Mukherjee and P. Thilagar, *Chem. Commun.*, 2016, **52**, 1070.

12 K. Nishino, H. Yamamoto, K. Tanaka and Y. Chujo, *Org. Lett.*, 2016, **18**, 4064.

13 H. Naito, K. Nishino, Y. Morisaki, K. Tanaka and Y. Chujo, *Angew. Chem. Int. Ed.*, 2017, **56**, 254.

14 H. Naito, Y. Morisaki and Y. Chujo, *Angew. Chem. Int. Ed.*, 2015, **54**, 5084.

15 A. Sakai, E. Ohta, Y. Yoshimoto, M. Tanaka, Y. Matsui, K. Mizuno and H. Ikeda, *Chem. Eur. J.*, 2015, **21**, 18128.

16 S. Kwon, K. R. Wee, Y. J. Cho and S. O. Kang, *Chem. Eur. J.*, 2014, **20**, 5953.

17 J. D. Chai and M. Head-Gordon, *Phys. Chem. Chem. Phys.*, 2008, **10**, 6615.

18 (a) X. Li, X. Tong, H. Yan, C. Lu, Q. Zhao, W. Huang, *Chem. Eur. J.*, 2016, **22**, 17282 (see Supporting Information); (b) J. Lu, H. Wan, Y. Xue, Y. Du, J. Lu, *Tetrahedron*, 2015, **71**, 7842.

19 A. Fukui, K. Hattori, Y. Hu, M. Shiotsuki, F. Sanda and T. Masuda, *Polymer*, 2009, **50**, 4159.

20 X. Zhan, A. Haldi, C. Risko, C. K. Chan, W. Zhao, T. V. Timofeeva, A. Korlyukov, M. Y. Antipin, S. Montgomery, E. Thompson, Z. An, B. Domercq, S. Barlow, A. Kahn, B. Kippelen, J.-L. Brédas and S. R. Marder, *J. Mater. Chem.*, 2008, **18**, 3157.

21 Gaussian 09, Revision B.01, M. J. Frisch, G. W. Trucks, H. B. Schlegel, G. E. Scuseria, M. A. Robb, J. R. Cheeseman, G. Scalmani, V. Barone, B. Mennucci, G. A. Petersson, H. Nakatsuji, M. Caricato, X. Li, H. P. Hratchian, A. F. Izmaylov, J. Bloino, G. Zheng, J. L. Sonnenberg, M. Hada, M. Ehara, K. Toyota, R. Fukuda, J. Hasegawa,

M. Ishida, T. Nakajima, Y. Honda, O. Kitao, H. Nakai, T. Vreven, J. A. Montgomery, Jr., J. E. Peralta, F. Ogliaro, M. Bearpark, J. J. Heyd, E. Brothers, K. N. Kudin, V. N. Staroverov, T. Keith, R. Kobayashi, J. Normand, K. Raghavachari, A. Rendell, J. C. Burant, S. S. Iyengar, J. Tomasi, M. Cossi, N. Rega, J. M. Millam, M. Klene, J. E. Knox, J. B. Cross, V. Bakken, C. Adamo, J. Jaramillo, R. Gomperts, R. E. Stratmann, O. Yazyev, A. J. Austin, R. Cammi, C. Pomelli, J. W. Ochterski, R. L. Martin, K. Morokuma, V. G. Zakrzewski, G. A. Voth, P. Salvador, J. J. Dannenberg, S. Dapprich, A. D. Daniels, O. Farkas, J. B. Foresman, J. V. Ortiz, J. Cioslowski, and D. J. Fox, Gaussian, Inc., Wallingford CT, 2010.